Utrecht University

Exploring the Physics and Emerging Clinical Applications of Quantitative Ultrasound in Oncology: A Comprehensive Review

Writing Assignment
MSc Medical Imaging

Pablo Xabier Arregui García

Examination Committee:

Examiner: Dr. Roel Deckers
Associate Professor, UMC Utrecht

2nd Reviewer: Dr. Clemens Bos
Associate Professor, UMC Utrecht

Utrecht, 18th September 2023

Exploring the Physics and Emerging Clinical Applications of Quantitative Ultrasound in Oncology: A Comprehensive Review

P.X. Arregui García
MSc Medical Imaging, Utrectht University

***Abstract*—Quantitative ultrasound (QUS) imaging aims at quantifying physical phenomena associated with the propagation of ultrasound in tissue, with the ultimate goal of determining the tissue microstructure. QUS techniques include attenuation evaluation, speed of sound evaluation, backscatter estimation, and envelope statistics. These techniques have been applied in multiple clinical applications such as liver steatosis, cervical ripening detection, bone properties assessment, and oncology. This study reviews the recent clinical applications of quantitative ultrasound with a special focus on oncology, as well as evaluates the current state of the implementation of QUS technology into clinical devices. The underlying physics of each quantitative ultrasound modality is explained in a comprehensive manner, and the aspects impeding the widespread clinical implementation of QUS are also investigated and discussed. Lastly, the potential of deep learning methods to enhance the accuracy, speed, and quality of quantitative ultrasound imaging is discussed.**

***Index Terms*—Ultrasound, Quantitative ultrasound, Speed of sound evaluation, Attenuation evaluation, Backscatter coefficient estimation, Envelope statistics**

1. INTRODUCTION

The field of medical imaging has experienced tremendous growth over the last 50 years [1], with the development of multiple imaging modalities. From the early days of X-ray radiographs to the development of MRI, all different imaging techniques have contributed to improving diagnostic and therapeutic medicine.

Among all the existing techniques, ultrasound has emerged as a versatile and indispensable tool. Unlike X-rays and Computed Tomography (CT), ultrasound imaging does not expose the body to harmful ionizing radiation, which has contributed to the widespread acceptance of this imaging modality. As a result of such an intrinsic safety profile, ultrasound imaging has become an essential diagnostic tool for vulnerable populations, such as children and pregnant women [2].

Furthermore, its portability and cost-effectiveness facilitated the spread of this imaging modality, making it more accessible than others (such as MRI) [3]. In addition, its real-time imaging capabilities have proved invaluable for guiding interventional procedures [4], enhancing precision in needle placements [5], and enabling dynamic assessments of organ function [6].

Despite all the aforementioned benefits, conventional ultrasound B-mode imaging is mainly qualitative, which limits its specificity. To overcome such a limitation, quantitative ultrasound (QUS) imaging aims at quantifying physical phenomena associated with the propagation of ultrasounds in biological tissue [7]. In QUS, the extracted information is used to produce a measurement of a global physical quantity within a region of interest (ROI) or parametric images for diagnosis. Thus, QUS has the potential to increase the specificity of image findings, leading to improvements in diagnostic ultrasound [8]. Moreover, QUS reduces system and operator dependency [8, 9], which is another favorable aspect of this technique.

In spite of the increasing presence of QUS in the literature, there is no clear consensus regarding the techniques considered as QUS. In their literature study, Oelze et al. [8] included flow estimation through Doppler, tissue elastography, and shear wave imaging as QUS techniques. On the other hand, more recent literature studies [7, 10] consider that the term "Quantitative" in QUS only refers to the specific field dedicated to biomarkers describing wave interactions with the insonified organs, in order to determine the tissue microstructure. As a result, in such studies, only attenuation, speed of sound, backscatter coefficient, and envelope statistics techniques are considered QUS (excluding flow estimation and elastography from this category). In our study, we will adopt this latter interpretation of QUS. It is also worth mentioning that both backscatter coefficient estimation and envelope statistics belong to backscatter imaging, and are consequently sometimes reported as sub-categories of such. However, in this work, we will treat them as distinct techniques, separating them into two different categories.

Several previous studies have reviewed the clinical applications of QUS imaging. In 2016 Oelze et al. [8] presented a survey of the clinical applications of backscatter coefficient estimation and envelope statistics-based techniques, and discussed the roadblocks to their implementation into clinical devices. However, this work only focused on backscatter imaging-based techniques and did not comment on the state of the art of the other QUS modalities. In 2021, two separate studies [7, 10] provided more recent overviews of QUS, not only including backscatter imaging, but also the rest of quantitative ultrasound methods. Nonetheless, these studies lacked an extensive discussion of the factors limiting the clinical implementation of quantitative ultrasound. A more

recent study by Fetzer et al [11], published in 2022, discussed the state of the art of attenuation, speed of sound, and backscatter coefficient estimation in the context of liver steatosis. Importantly, this study also discussed challenges and provided recommendations for the clinical translation of quantitative ultrasound. Nevertheless, it did not include advances regarding envelope statistics and was focused solely on liver steatosis, leaving out other clinical fields in which QUS can be applied (such as oncology). Thus, to the best of our knowledge, there is no recent study providing the state of the art of all existing QUS techniques, while discussing the roadblocks and limitations to the applicability in the clinic, in other fields rather than liver diseases.

Taking into account all of the aforementioned, in this study, we will provide a recent review of the state of the art in quantitative ultrasound, focusing on all QUS techniques (attenuation, speed of sound, backscatter estimation, and envelope statistics). The underlying physics of each technique will be explained, recent (when possible) clinical studies will be reviewed, and the state of the implementation of each method in the clinic will be analyzed. Although quantitative ultrasound has a wide range of clinical applications, including quantifying liver steatosis [9], detecting cervical ripening [12], and assessing bone properties [13], this literature review will concentrate on QUS applications in oncology. Furthermore, the limitations and current obstacles to the widespread implementation of QUS into clinical practice will also be discussed. Finally, we will evaluate the future directions of this technique, including the potential of Deep Learning methods to enhance the accuracy, speed, and quality of quantitative ultrasound imaging.

2. PHYSICS OF ULTRASOUND

Before delving into the different existing QUS techniques, in this section, we will introduce some basic concepts regarding acoustic wave propagation, ultrasound image formation, and factors modulating the ultrasound image.

2.1. Acoustic waves and propagation

Compression (or longitudinal) waves alternate compressions and rarefaction of tissue in the direction of propagation of the wave [7], and are used in all ultrasound imaging modes (grayscale, Doppler, elastography, and QUS). The velocity of propagation of these waves is known as the speed of sound (SoS) and it is a tissue-dependent magnitude.

When compression waves propagate through biological tissue, they undergo various physical phenomena. These include alterations in their direction and amplitude, which can occur as a result of reflection or refraction at interfaces between media with distinct acoustic impedances (determined from the speed of sound and tissue mass density). Additionally, these waves may experience a reduction in amplitude, a phenomenon referred to as attenuation, caused by absorption and scattering within the medium [7].

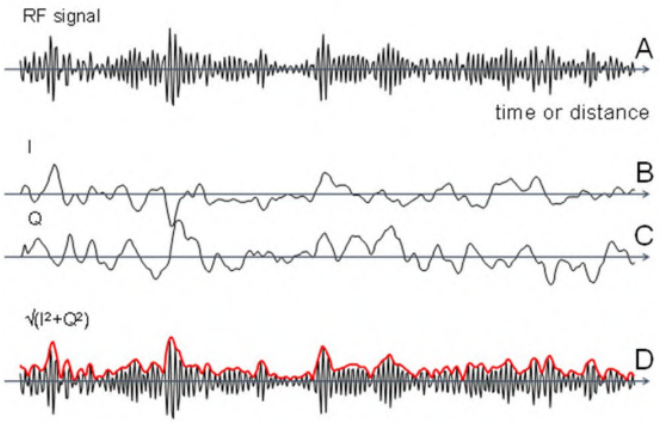

Fig. 1: RF signal processing and ultrasound image formation [7]. **A**: RF signal. **B** and **C**: I and Q demodulated components. **D**: RF echo envelope.

2.2. B-mode image formation

Despite the tissue-dependency of the speed of sound, the propagation speed of acoustic waves is assumed to be constant in ultrasound systems, with a typical value of 1540 m/s, which is used to convert time into distance and generate an image. That is, the systems measure the time difference between the emission and reception of echoes and rely on the fixed speed of sound to precisely map the acquired echoes into depth.

The process of ultrasound B-mode image formation (depicted in Fig. 1) starts with radiofrequency (RF) data processing [7]. The time domain RF signal contains detected reflected and scattered echoes returning to the transducer. To create B-mode images, the RF signal is first processed to obtain the demodulated in-phase (I) and quadrature (Q) components. Next, the RF echo envelope is obtained as the square root of I^2 plus Q^2. Finally, the image is created by mapping the magnitude of the echo envelope in grayscale, representing B-mode speckle at a given lateral (RF scan line) and depth (time).

2.3. Point spread function and wave interferences

The speckle in ultrasound imaging refers to the granular pattern that appears in B-mode images. This pattern (and hence the ultrasound B-mode image) is mainly modulated by two factors: the point spread function (PSF) and wave interferences.

PSF

The speckle in B-mode images provides a signature of the tissue microstructure at a resolution determined by the system's point spread function [7]. When backward ultrasound waves emitted by a point source (e.g. a cell) are detected by the probe, they are filtered by the PSF of the ultrasound system, causing blurring. This blurring (which is a result of the limited resolution of the system, combined with probe characteristics and scanner settings) does not allow to resolve the geometry of tiny objects or distinguish two objects that are closely located. Thus, the PSF impedes resolving the tissue microstructure and

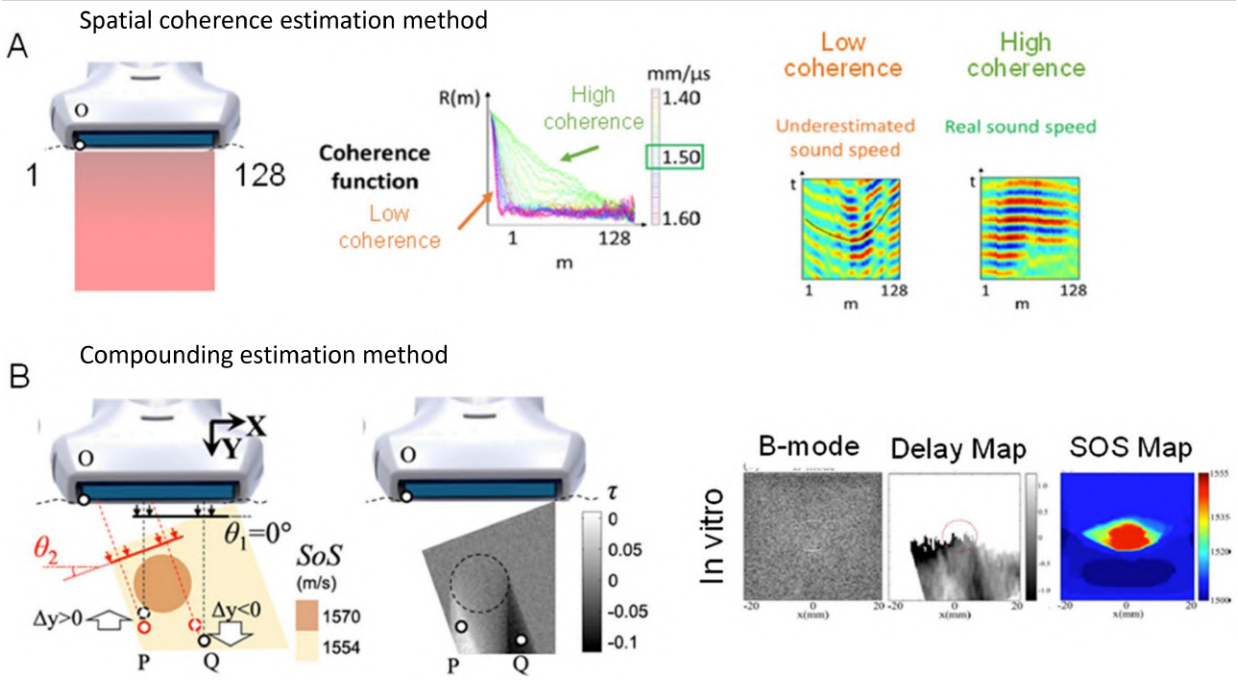

Fig. 2: Spatial coherence (**A**) and compounding (**B**) SoS estimation methods [7]. **A**: The spatial coherence method employs the coherence factor to estimate the SoS. A tissue with low coherence among transducer elements location underestimates the speed of sound, whereas a tissue with high coherence provides the real value of the SoS. **B**: The compounding method estimates the SoS by insonifying the tissue at different angles. More details about this method can be found in [14].

contributes to the speckle pattern that is observed in B-mode images.

Wave interferences

When ultrasound waves interact with tightly packed tissue components, constructive and destructive wave interferences originate [7]. Such interferences happen due to the presence of numerous reflectors and they contribute to the speckle pattern features. Thus, the reflectors' number and location are significant factors that determine the characteristics of the speckle image and provide important sub-resolution information gathered by QUS backscatter imaging biomarkers (which will be discussed later in sections **3.3** and **3.4**).

3. QUS TECHNIQUES

QUS uses ultrasound waves to extract fundamental properties of tissues by analyzing their interaction with the tissue microstructure [7]. There are four techniques used in QUS: speed of sound evaluation, attenuation coefficient evaluation, backscatter coefficient estimation, and envelope statistics. Each of these methods is used to extract parameters related to tissue microstructural properties. In this section, for each technique, we will first provide an overview of the underlying physics, followed by the different measurement methods employed, and the parameters that can be extracted. Then, we will review recent (if possible) clinical studies employing QUS in oncology and evaluate the extent to which each method has been implemented in clinical devices.

3.1. Speed of Sound Evaluation

3.1.1. Overview

As mentioned earlier, clinical US systems assume a constant speed of sound (1540 m/s) along the whole path that the ultrasound waves travel, which is used to estimate the depth at which objects are located. However, different tissues may have different speed of sound (SoS) values (in soft tissues, it varies up to 10% with respect to the assumed value [7]), violating the previous assumption and causing image quality degradation (due to the wrong depth estimation of objects). Original efforts in the field of speed of sound imaging were precisely directed at improving the quality of B-mode images affected by this phenomenon [15], locally adjusting the speed of sound to reduce blurring. These early efforts were later applied in the field of QUS, where tissue-dependent variations in SoS are retrieved and can be used as a biomarker of a pathological state.

3.1.2. Measurement

There are three main methods to quantify SoS: focusing, spatial coherence, and compounding.

Focusing method

The focusing method consists of varying the speed of sound in the ultrasonic beamformer until the quality of the image is maximized [16]. To evaluate the image quality, options such as echo signal amplitude, minimum entropy, or lateral resolution can be used [10]. This method's advantage is

its ease of implementation as it can use existing hardware configurations of diagnostic equipment. However, the focusing method is time-consuming, due to the requirement of multiple scans. Furthermore, this method only provides a mean estimate along the ultrasound beam and lacks the ability to produce a local measure within a given ROI of an organ having inhomogeneous SoS.

Spatial coherence method

The spatial coherence method (Fig. 2.A) employs the coherence factor to estimate the actual speed of sound. The coherence factor can be used as a measure of image quality [17], and the sound speed corresponding to a specific region of tissue is estimated by maximizing the coherence factor [18]. This method provides a global value of the SoS in the selected ROI in m/s, without a parametric image. The advantage of this method is its high estimation accuracy, combined with the flexibility to adjust the area where the SoS is calculated (this was not possible in the focusing method), which can be set locally or globally [10]. However, the shortcoming is that it requires individual control and signal processing for each element in the probe, which makes it more hardware-restrictive than focusing methods.

Compounding method

The compounding method (Fig. 2.B) directly evaluates the speed of sound by comparing spatial shifts in images from different transmission and reception angles [10, 14]. If the mismatch between the assumed SoS for beamforming and the actual SoS is high, it can cause spatial errors due to changes in the path length at different angles. To minimize the difference between the assumed and actual speeds of sound, the magnitude and direction of the shift are optimized [19]. Contrary to the previously discussed methods, the compounding method provides a parametric map of the SoS in the selected ROI, although it suffers from a lack of robustness.

3.1.3. Clinical applications

In the context of oncology, speed of sound imaging QUS techniques have been used for breast cancer assessment. The use of SoS imaging in this field had its origin in 2007, when Duric et al. [20] presented an ultrasound tomography system that combined both reflection and transmission imaging, and allowed the estimation of the speed of sound and attenuation coefficient. Employing such a system, in 2009, Li et al. [21] performed a speed of sound analysis on breast datasets. In this study, they found significant differences in SoS between malignant and benign lesions and suggested that sound-speed tomograms could be used to differentiate breast lesions, assess breast cancer risk, and evaluate the clinical response of breast cancer patients to chemotherapy. A few years later, Duric et al. [22] investigated the use of whole breast sound speed measurement as a marker of breast density (which is a known risk factor for breast cancer). They showed that volume-averaged sound speed was significantly correlated to mammographic percent density, showing the viability of the speed of sound to measure breast density and its potential for early assessment of breast cancer risk. In a more recent study (2019), Wiskin et al. [23] presented an algorithm that used the estimated speed of sound for the calculation of breast density. Later that year, Ruby et al. [24] investigated the feasibility of SoS ultrasound to distinguish breast cancer from fibroadenoma and healthy tissue, demonstrating the speed of sound evaluation's capabilities for the differentiation of solid breast lesions. Importantly, in contrast to the previously presented studies, this work employed a conventional ultrasound system and not a tomography system.

Besides its applications in breast cancer, SoS techniques have been investigated for prostate cancer assessment. In their study, Tanoue et al. [25] measured the speed of sound of prostatic tissue to assess malignancy. They determined that the prostatic cancer tissue type could be classified by employing speed of sound imaging techniques. In a later study, Seifabadi et al. [26] characterized healthy and malignant prostate cells employing speed of sound QUS techniques, and correlated SoS maps with T2-weighted MRI and pathology findings. Other than breast and prostate cancer, there are not many other oncology-related applications of SoS imaging in the literature, being this technique especially prominent in the field of liver diseases.

3.1.4. Clinical implementation

SoS estimation capabilities have been implemented into several ultrasound tomographic systems. Some systems that are currently being used to perform in vivo clinical tests are the SoftVue (Delphinus Medical Technologies), QT Scanner 2000 (QT Ultrasound), MUT Mark II (Mastoscopia), and KIT 3D USCT (Karlsruhe Institute of Technology) [27]. However, all these examples correspond to ultrasound tomography systems that are exclusively built for breast cancer treatment (see Fig. 3). In addition to those systems, a few ultrasound manufacturers are offering SoS estimation capabilities [7], which are mostly based on the calculation of the mean speed of sound within a selected ROI (without providing SoS maps). An example of such a system is the Aixplorer MACH 30 (Aixplorer, Supersonic Imagine) [28].

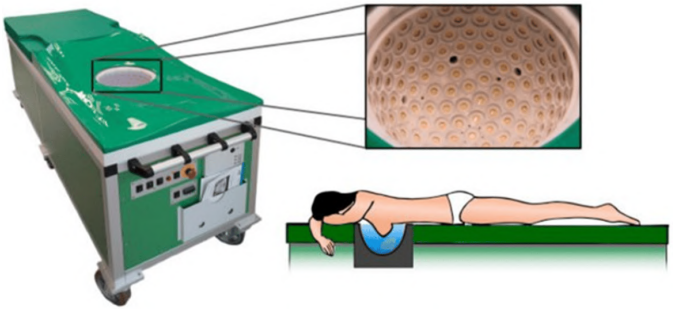

Fig. 3: KIT 3D USCT ultrasound tomography system designed by Karlsruhe Institute of Technology [27].

3.2. Attenuation Coefficient Evaluation

3.2.1. Overview

Ultrasound attenuation refers to the loss of mechanical energy as an acoustic wave propagates in tissue [29]. Due to the attenuation, the magnitude of the echo within the image is reduced, which can lead to a loss of structural details in deeper areas and the appearance of shadows. As a result, attenuation can be seen as either an artifact in imaging or a unique characteristic of the tissue that has diagnostic value. QUS focuses on the latter aspect, utilizing attenuation to characterize tissue.

Attenuation increases with ultrasound frequency, and it is usually reported in dB/cm/MHz. This relation between attenuation and frequency is often assumed to be linear on a log scale [30]. Thus, the attenuation at a given frequency can be obtained by multiplying the attenuation in dB/cm/MHz by the corresponding frequency (MHz). This results in an attenuation measurement in dB/cm, which is often used. Another value that is usually measured and reported is the slope of the linear relation between attenuation and frequency, which is known as the attenuation coefficient slope (ACS) [30].

3.2.2. Measurement

To determine the attenuation characteristics of the target tissue, one can evaluate the backscattered signal that returns in the same direction as the transmission. Based on this, two techniques are mainly used to measure attenuation, i.e., the spectral difference and the spectral shift methods.

Both methods start with the discretization of an ROI into rectangular windows (Fig. 4.A) to locally estimate the attenuation coefficient. In the spectral difference method (Fig. 4.B), the attenuation coefficient slope is estimated from the reduction of the echo signal power with depth, obtained by comparing the signal from windows at two different depths. On the other hand, the spectral shift method (Fig. 4.C) estimates the ACS from the downshift in the center frequency of the backscatter echo with depth, which happens due to frequency-dependent attenuation. This second method assumes a linear relation between frequency and attenuation, which is not completely accurate for many tissues [7].

Furthermore, these methods require some calibration to account for the wave diffraction confounder of the transducer [7], a phenomenon that reduces the echo signal power with depth. To perform the calibration, echo signals from a reference phantom whose attenuation is known must be obtained using the same equipment and system settings as the clinical examination. After the calibration, the attenuation coefficient of the scanned organ at the frequency and depth of interest is finally retrieved.

3.2.3. Clinical applications

The clinical applications of attenuation coefficient evaluation in the field of oncology mainly involve breast, prostate, and thyroid cancer. Regarding breast cancer, as mentioned before in section **3.1.3**, in 2007 the ultrasound tomography system was presented, which had both attenuation and speed

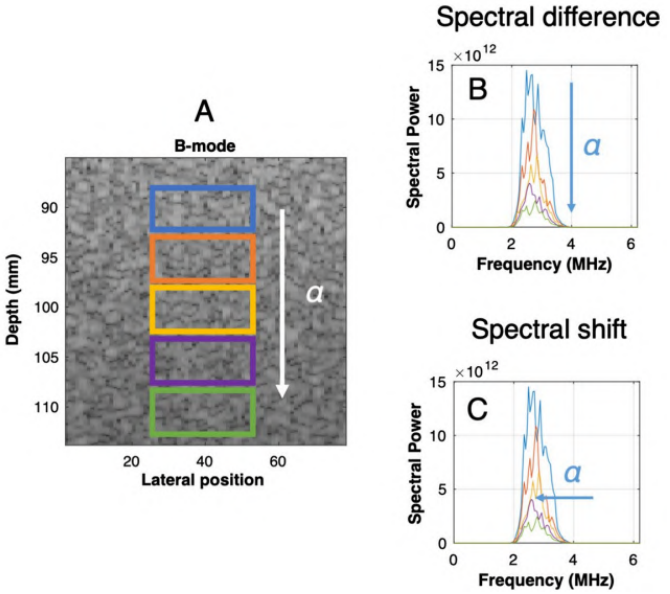

Fig. 4: Attenuation coefficient estimation methods. **A**: Division of the ROI into rectangular windows for local attenuation coefficient calculation. **B**: Spectral difference method. **C**: Spectral shift method. The figure was obtained from [7].

of sound imaging capabilities. However, despite the authors in [20] highlighting the potential of combining both speed of sound and attenuation information for characterizing benign and malignant lesions, only Wiskin et al. [23] employed both biomarkers in their study for the calculation of breast density. Additionally, another recent work by Pal et al. [31] used attenuation coefficient evaluation combined with near-infrared spectroscopy for breast tissue characterization, demonstrating that cancerous tissue presented a higher attenuation coefficient compared to normal tissue.

Concerning prostate cancer, an early study by Chapelon et al. [32] in 1999 investigated the use of attenuation imaging during the treatment of localized prostate cancer through HIFU. They determined that real-time visual display of the damaged tissue via differential imaging of the attenuation coefficient could provide the surgeon with an instant assessment of the treatment's result. Besides this study, and despite the potential of the attenuation coefficient for tumorous tissue characterization, there are no recent studies (to the best of our knowledge) employing the attenuation coefficient as a biomarker to distinguish pathological from healthy tissue in prostate cancer.

With respect to thyroid cancer, a study by Zenteno et al. [33] in 2013 successfully characterized different types of thyroid tissue employing attenuation coefficient estimation techniques in rodent models. In 2015, Rouyer et al. [34] investigated the variability of ultrasonic attenuation coefficients in healthy thyroids, finding a non-negligible inter-subject variability. Some years after, in 2017, Coila et al. [35] validated the feasibility of in vivo estimations of the attenuation coefficient slope (ACS) from thyroid nodules, and found that all thyroid nodules

had a lower ACS with respect to healthy tissue. Despite all these efforts, not many recent studies employing attenuation coefficient estimation techniques to characterize thyroid tissues can be encountered. Nonetheless, as with SoS, attenuation imaging is especially relevant in the field of liver diseases.

3.2.4. Clinical implementation

All ultrasound tomographic systems that were listed in section **3.1.4** combine speed of sound and attenuation capabilities. However, as commented before, the applicability of those systems is only limited to breast cancer. Apart from those systems, few ultrasound manufacturers offer real-time attenuation images on their scanners. Examples of such scanners are the Aplio i-series US systems (Cannon Medical Systems, Fig. 5) [36], FibroScan system (Echosens) [37], and RS85 US system (Samsung Medison) [38]. Nevertheless, the attenuation coefficient estimation capabilities of these systems have been employed for liver diseases, and no use of them in oncology has been reported.

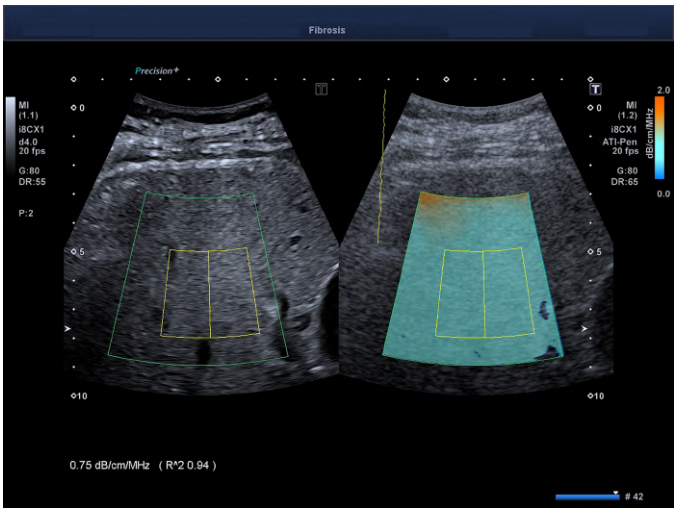

Fig. 5: Attenuation coefficient estimation in a Aplio i800 US system [37].

3.3. Backscatter Coefficient Estimation

3.3.1. Overview

Backscatter imaging refers to the analysis of echoes received by an ultrasound transducer caused by compression wave reflection and scattering. These echoes are affected by the tissue microstructure, resulting in changes in magnitude due to constructive and destructive wave interferences.

In the field of QUS imaging, the most widely accepted method for describing backscatter is to use the magnitude squared and frequency dependence of RF echoes to calculate the backscatter coefficient (BSC) [7]. The BSC at a particular frequency corresponds to the time-average scattered intensity in the backward direction per unit solid angle per unit volume, normalized by the average incident wave intensity ($cm^{-1}Sr^{-1}$) [29]. In addition to being related to tissue microstructure, the BSC is a fundamental property of tissue, which makes it both

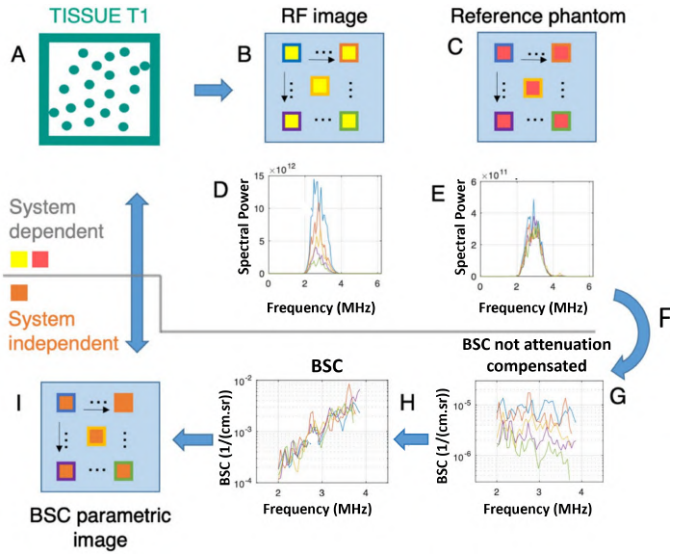

Fig. 6: Reference phantom method for the estimation of BSC [7]. **A**: The tissue is interrogated with ultrasound. **B**: RF image obtained from backscattered ultrasound. **C**: Reference image obtained from the reference phantom. **D** and **E**: The computed power spectrum at each window for both images. **F**: The spectral ratio is computed and a calibration by the known BSC of the reference phantom is performed to eliminate system-dependent effects. **G**: BSC affected by total attenuation. **H**: BSC after removal of depth-dependent attenuation. **I**: Resulting BSC parametric image.

operator and system-independent. BSC estimation-based QUS techniques consist of parameterizing the BSC to yield estimates of the scatterer properties, which provide a geometrical interpretation of the underlying tissue microstructure.

3.3.2. Measurement

The BSC is most commonly obtained using the reference phantom technique [7], following the process depicted in Fig. 6. First, the tissue is interrogated and a backscattered RF image is obtained, after which the image is divided into discrete rectangular windows. Next, using the same ultrasound system, a reference RF image is taken, employing a reference phantom with known BSC. This reference image is then divided into the exact same windows as before. Subsequently, at every measurement window, power spectra are computed for both images. Then, to eliminate the effects caused by the point spread function and beam diffraction, a spectral ratio is computed at each window, performing a calibration by the known BSC of the reference phantom. However, the tissue BSC is still affected by total attenuation, which is why depth-dependent attenuation is removed for every window. After the compensation for attenuation, a system-independent BSC parametric image is finally obtained.

The reference phantom technique has the benefit of being applicable for any transducer geometry [8]. In addition to this technique, there is another BSC estimation method called the planar reference method, which employs a smooth plate

of material with known reflectivity instead of a phantom to provide the reference signal. However, the utilization of this technique is limited to weakly focused single-element transducers, which makes it less versatile than the reference phantom approach.

3.3.3. Parameters

In the previously presented QUS techniques (speed of sound and attenuation coefficient) the tissue property being measured was directly used as a QUS biomarker of pathological state. However, BSC-based QUS techniques do not infer tissue properties directly from the BSC, but they consist of parameterizing the measured BSC and employing those parameters to estimate microstructural tissue properties.

An early approach to parameterizing the BSC consisted of fitting a line to the normalized power spectrum converted to decibel scale versus frequency. In this approach, presented by Lizzi et al. [39], the spectral slope (SS), mid-band fit (MBF), and spectral intercept (SI) were used to parameterize the normalized power spectrum, and these parameters were then used to describe the tissue microstructure.

Nevertheless, the linear approach may fail to capture all of the structure in the normalized power spectrum or the BSC representing scattering from tissues [8]. As a result, an alternative approach was developed, which consisted of modeling the BSC using an intensity form factor [40]. Such intensity form factor models yield tissue microstructure-related parameters like the effective scatterer diameter (ESD) and the effective acoustic concentration (EAC).

3.3.4. Clinical applications

Compared to SoS and attenuation estimation, Backscatter coefficient estimation techniques have been extensively applied in the field of oncology. As a result, in this section, we will mainly focus on recent applications. Specifically, applications have been especially reported in the fields of breast cancer, prostate cancer, thyroid cancer, and lymph nodes.

Breast cancer

There are multiple recent studies employing BSC-derived parameters as biomarkers for breast tissue characterization. Sadegui et al. [41] evaluated the efficacy of applying textural analysis techniques to QUS spectral parametric maps to classify malignant and non-malignant breast lesions. Following a similar trend, Nizam et al. [42] employed QUS parameters (ESD) for binary classification of breast lesions. They highlighted the promising capabilities of using ESD for lesion binary classification, achieving high sensitivity, specificity, and accuracies of around 96% in each case. Besides tissue characterization, BSC estimation has been recently used to evaluate treatment response. An example of such an application is the study by Bhardwaj et al. [43], which explored the capabilities of QUS spectral parameters to predict the recurrence of locally advanced breast cancer in the early stages of neoadjuvant chemotherapy. By employing multiple QUS parameters and applying textural analysis techniques, the authors demonstrated the effectiveness of QUS in predicting recurrence.

Prostate cancer

Treatment response assessment has been one of the recent applications of BSC estimation techniques in the field of prostate cancer. The study by Sharma et al. [44] is an example of this application. In such study, the authors examined prostate tumor response to ultrasound-stimulated microbubbles (USMB) and hyperthermia (HT) in mice, using multiple BSC-related parameters, such as the spectral slope, spectral intercept, mid-band fit, average scatterer diameter, and average acoustic concentration. Their findings revealed the usefulness of such parameters for assessing tumor response to treatment in vivo. Another study by Rohbach et al. [45] used five spectral parameters to improve transrectal ultrasound (TRUS) guided biopsies, directing them to cancer-suspicious regions in the prostate.

Thyroid cancer

Some recent studies have employed BSC techniques in the field of thyroid cancer. Rohrbach et al. [46] employed parameters like the EAC, ESD, and other spectral parameters to detect thyroid cancer. By training a linear classifier with combinations of such parameters, the authors successfully developed a non-invasive tool that could potentially be used for thyroid cancer detection. In a similar study, Goundan et al. [47], investigated the use of multiple BSC-derived parameters to distinguish between benign and malignant thyroid nodules. Similarly to the previously presented study, the authors trained a linear classifier employing the estimated QUS parameters, concluding that QUS has the potential to improve the discrimination between benign and malignant thyroid nodules, and hence reduce the number of biopsies of benign nodules.

Lymph nodes

Tran et al. [48] employed quantitative ultrasound radiomic markers to predict radiotherapy response in metastatic lymph nodes of head and neck cancer. Six QUS parameters were extracted, parametric maps were formed and textural analysis was applied on such parametric maps. The authors found statistically significant differences in QUS-radiomic parameters between complete and partial chemotherapy responders, determining that multivariable QUS-radiomic features have the capacity to predict treatment response. In a more recent study, Hoerig et al. [49] aimed to apply BSC estimation methods to differentiate metastatic and non-metastatic lymph nodes in vivo, employing clinical frequencies to achieve this. This study determined that metastatic lymph nodes in vivo exhibit significant differences in ESD and EAC compared with their non-metastatic counterparts, with the subsequent potential to aid in the identification of lymph nodes during biopsies and avoid unnecessary invasive procedures.

3.3.5. Clinical implementation

To the best of our knowledge, no ultrasound manufacturer has yet released a clinical system with BSC estimation capabilities. Nevertheless, in [50], a commercial implementation

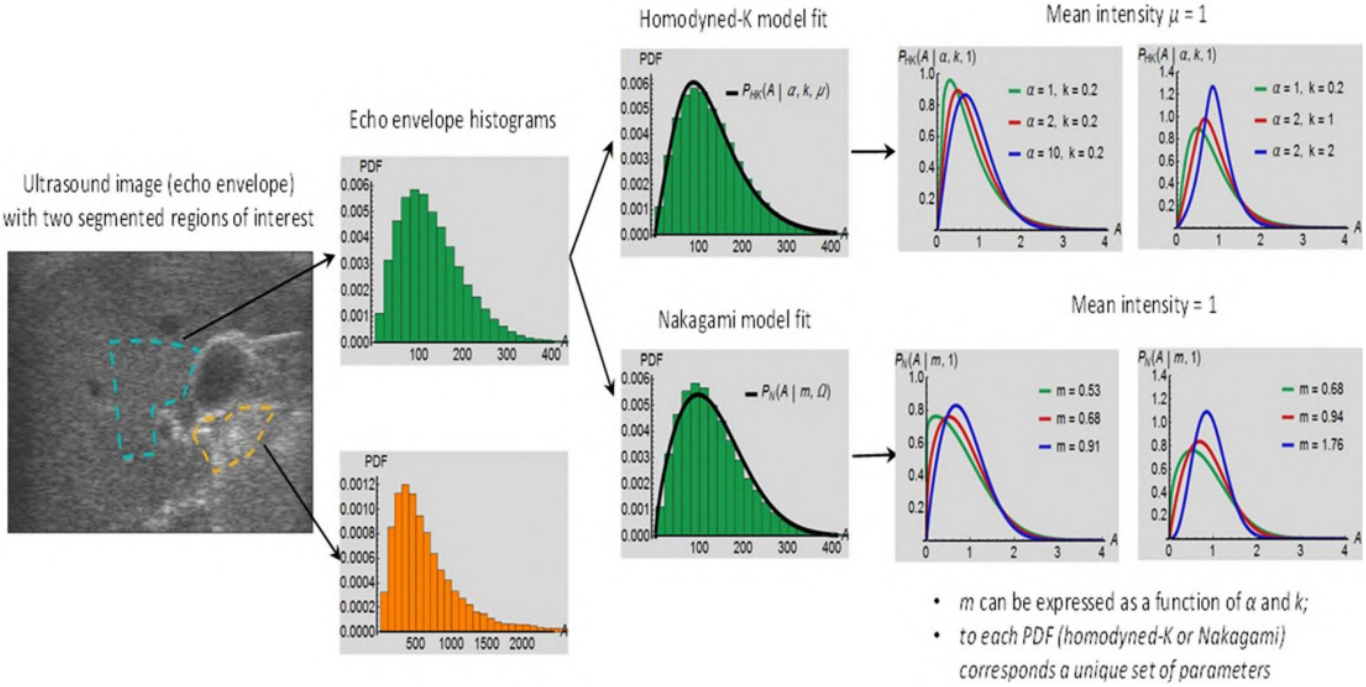

Fig. 7: Echo envelope statistics histogram fit using homodyned K and Nakgami statistical models [7].

of BSC estimation was presented, showing that it is feasible to measure the BSC with a clinical scanner in a specified ROI by having pre-acquired phantom data in the ultrasound system. Considering the number of studies using BSC-related parameters and its minimal system dependence, it is expected that BSC calculation will be incorporated into clinical systems in the future.

3.4. Envelope Statistics

3.4.1. Overview

In addition to the BSC, the RF echo envelope of the backscattered ultrasound also contains information about the underlying tissue microstructure. Envelope statistics consists precisely of exploiting first-order statistical properties of such an envelope to infer the microstructural properties of tissue. In contrast to the BSC estimation techniques, which convert backscattered signals into the frequency domain, envelope statistics techniques mainly work in the time domain (same as classic B-mode imaging).

3.4.2. Measurement

As explained in section **2.2**, B-mode images are formed using the magnitude of the RF echo envelope (or speckle). Taking this into account, in envelope statistics, an ROI of the B-mode image is selected, and a histogram of the echo envelope magnitude is computed. Next, probability density functions of statistical models are used to fit the histogram, and the parameters corresponding to those statistical models are employed to infer tissue properties. This process is depicted in Fig. 7.

3.4.3. Distributions and parameters

Multiple distributions can be used to describe the magnitude of the echo envelope, and each distribution adjusts to certain scattering characteristics.

Rayleigh and Rician distributions

The most basic distribution is the Rayleigh distribution, which arises when a large number of nearly identical and random scatterers contribute to the echo signal [8]. Pre-Rayleigh scattering conditions occur when this number of scatterers per resolution is low (less than 10). The Rician distribution is an extension of the Rayleigh distribution, and it provides an estimate of the strength of coherent signal. It models a situation where there are specular scatterers or these are periodically located. These two distributions provide hints of the scatterers' distribution but do not include any quantitative parameter. Nevertheless, other distributions introduce parameters related to tissue characteristics.

K distribution

The K distribution [51] is a generalization of the Rayleigh distribution that can be used in situations where the number of scatterers per resolution is small. This distribution introduces the parameter μ, which corresponds to the number of scatterers per resolution cell (when $\mu \to \infty$ the K distribution approaches the Rayleigh distribution).

Homodyned-K distribution

The homodyned-K [52] is an extension of the K distribution. Besides the capabilities of its counterpart, this distribution can model situations where coherent signals exist due to periodically located scatterers. In addition to μ, the homodyned-K

distribution includes a second parameter k, which describes the level of structure or periodicity in scatterers' locations.

Nakagami distribution

The Nakagami distribution [53], or m-distribution, introduces the Nakagami parameter m. Depending on the value of m, the signal (or tissue) can be classified into four categories [8]: 1) $m < 0.5$, few scatterers per resolution cell with gamma-distributed scattering cross sections; 2) $0.5 \leq m \leq 1$, pre-Rayleigh scattering conditions; 3) $m \approx 1$, Rayleigh distributed; 4) $m > 1$, the distribution is considered Rician or post-Rayleigh. This distribution is highly versatile as it is applicable in multiple cases.

3.4.4. Clinical applications

Similarly to BSC, envelope statistics techniques have been used for breast cancer, prostate cancer, thyroid cancer, and lymph nodes.

Breast cancer

In 2003, Shankar et al. [54] used a multiparametric approach for the classification of breast masses in ultrasound images. These parameters were based on Nakagami and K distributions that were fitted to the echo envelope, which were combined to create a linear discriminant that successfully distinguished malignant and benign masses. Examples of similar approaches can be found in the recent literature. For instance, Muhtadi et al. [55] extracted texture features from Nakagami parametric maps generated from ultrasound envelope images to classify breast cancer. They demonstrated that texture features derived from Nakagami parameters have the potential to early diagnose breast cancer. A similar study by Chowdhury et al. [56] analyzed Nakagami parametric maps for the classification of breast lesions. The particularity of this study is the extraction of numerous features (up to 72), which were used to conduct a thorough feature selection, determining those that are more useful for the classification of breast cancer.

Prostate cancer

Some recent studies reported the use of envelope statistics in the field of prostate cancer. In their study, Rohrbach et al. [45] (already introduced in section **3.3.4**) combined the use of BSC-derived parameters and the Nakagami parameter to train a linear discriminant classifier and a support vector machine, in an attempt to improve the detection of prostate cancer. The best result was reported when combining envelope statistics with prostate-specific antigen values and BSC-specific parameters (EAC and ESD). Similarly to the previous study, Xiao et al. [57] attempted to improve the detection of prostate cancer by extracting spatial features from Nakagami distribution mean diagrams and training a support vector machine.

Thyroid cancer

Montero et al. [58] evaluated the performance of a QUS-based multi-parametric classification technique to distinguish between benign and malignant thyroid cancer in rodent models. In such a study, they employed a combination of attenuation coefficient slope, ESD, EAC, Nakagami parameter, and k-parameter to perform a binary classification with a linear discriminant classifier. They determined that the best performance was achieved when combining EAC and Nakagami parameters, resulting in a sensitivity and specificity of 100%. In a more recent study of similar characteristics, Goundan et al. [47] trained a linear discriminant classifier for the classification of benign and malignant thyroid tumors, combining different BSC-related parameters with the Nakagami parameter.

Lymph nodes

Mamou et al. [59] utilized a combination of backscatter and envelope parameters for freshly dissected lymph node characterization in patients with colorectal cancer. The study used both Nakagami and homodyned-K distribution to parameterize the echo envelope in a 3D high-frequency ultrasound. By combining the effective scatterer size with homodyned-K distribution parameters, the authors achieved a specificity and sensitivity of 95%, proving the usefulness of this technique for detecting small metastatic foci in dissected lymph nodes. Another study by Bui et al. [60] attempted to identify the probability density functions that best model the envelope of lymph node parenchyma, fat, and phosphate-buffered saline (PBS). After a comparison of nine distributions (including Rayleigh and Nakagami), the Gamma distribution was found to be the best to model parenchyma, while the Weibull distribution was determined to be the optimal choice for fat and PBS.

3.4.5. Clinical implementation

An example of envelope statistics implementation in clinical devices is the acoustic structure quantification (ASQ) software included by Toshiba in their Aplio ultrasound scanners [61]. The ASQ technique statistically analyzes the echo signals and quantifies the degree of deviation from the Rayleigh distribution. However, this technique has been mainly used for liver diseases and its use in oncology is still to be investigated. Furthermore, this software employs only the Rayleigh distribution without providing any other statistical model parameter (such as Nakagami or K-distribution).

4. LIMITATIONS TO CLINICAL IMPLEMENTATION AND WIDESPREAD USE

Quantitative ultrasound techniques have emerged as an alternative to conventional B-mode imaging, providing quantitative biomarkers that improve diagnostic capabilities. However, their implementation into clinical practice in oncology has not been straightforward.

On the one hand, speed of sound and attenuation imaging have been available in several manufacturers´ systems for years. An example of such a system is the ultrasound tomography device used for breast cancer assessment. However, this system's utility is limited to breast cancer assessment alone, making it less versatile and cost-effective compared to conventional ultrasound systems. Moreover, beyond breast cancer, research on the application of SoS and attenuation coefficient estimation in oncology remains relatively scarce. Thus, despite the implementation of these biomarkers in

multiple commercial devices, due to a lack of recent studies employing them for cancerous tissue characterization or therapy response assessment, their clinical use for oncology is unclear at the moment.

On the other hand, for backscatter coefficient and envelop statistics, the picture is rather different. Multiple recent studies are reporting the use of these techniques in oncology, showing their validity for improving diagnostics, but their integration into clinical systems has been limited so far. In the past, this constraint was attributed to the lack of accessibility to ultrasound RF data. However, in model digital scanners, this challenge has been largely overcome, as RF data can be easily accessed. Previous studies [8] also highlighted the need for a proper calibration procedure in order to use BSC-based QUS techniques, which is more likely to be the reason behind its cumbersome clinical implementation. However, the pre-calibration burden would be greatly reduced if manufacturers included pre-collected data from reference phantoms in their ultrasound systems [7, 8].

In general, we consider that the main limitation for the actual widespread implementation of QUS techniques in oncology is the need for standardization. In the field of liver diseases, such standardization is currently an ongoing process, performed by the QIBA-PEQUS (quantitative imaging biomarkers alliance–pulse echo quantitative ultrasound) committee of the Radiological Society of North America [11]. This committee aims to establish a consensus on standardized quantitative ultrasound features for hepatic steatosis biomarkers, to be used under equivalent conditions across manufacturers. To achieve this, they presented a three-level framework, which consisted of: 1) establishing measurement standards to reduce variability and bias; 2) demonstrating how a specific biomarker is related to the biological concept of interest; 3) investigating the relationship between multiple simultaneous biomarker measurements and the biologic concept of interest (combining SoS, attenuation coefficient, and BSC). Therefore, following the demonstration of several studies indicating that QUS has the potential to improve cancer diagnostics and treatment, a similar effort for standardization in the field of oncology would be of utmost importance. This process would offer valuable insights into the real-world applicability of less commonly employed biomarkers (in oncology) such as SoS or attenuation coefficient, as well as facilitate the transition of BSC and envelope statistics from research settings to clinical practice.

5. FUTURE DIRECTIONS: QUS AND DEEP LEARNING

Despite the challenges that need to be tackled for the clinical implementation of QUS, the field continues evolving and new applications are emerging. In this aspect, artificial intelligence (AI) has started to make an impact in QUS. In particular, there are two main applications for which AI has been used in QUS.

On one side, multiple studies have reported the use of machine and deep learning approaches for feature extraction from QUS multi-parametric images [62, 63]. In those studies, especially prominent for breast cancer, multiple BSC and envelope statistics-related parameters are used for parametric map creation, which are then analyzed with deep learning to extract relevant features used for tissue characterization or therapy response assessment.

On the other side, several studies have employed deep learning for speed of sound image reconstruction, allowing SoS estimation in conventional ultrasound scanners [64, 65]. Solving the reconstruction problem to obtain such SoS maps in conventional ultrasound scanners is a challenging task that requires carefully chosen regularization and numerical optimization techniques, but the implementation of deep learning-based methods eases the task of finding the best regularization parameters.

All in all, the use of AI in QUS is starting to have a significant impact, and the relevance of machine and deep learning in this field is expected to grow in the following years, as AI-based approaches become more and more popular. AI could potentially tackle the limitations to the widespread use of quantitative ultrasound that were previously mentioned, allowing the reconstruction of the speed of sound maps and facilitating the implementation of automatic tissue characterization software in conventional ultrasound scanners based on QUS biomarkers.

6. CONCLUSION

Quantitative ultrasound is an innovative technique that shows great promise in revolutionizing the diagnosis and treatment of various diseases. By correlating quantitative biomarkers to the biological state of tissues, QUS has been the focus of numerous clinical applications. In this work, we have focused on QUS applications in oncology, providing the physics and reviewing the use of each QUS technique in this field. From this study, it is clear that BSC estimation and envelope statistics are the most promising and commonly used QUS techniques in the field of oncology, given the multiple tissue-describing biomarkers that they provide. However, despite their potential, these techniques are not yet available in clinical systems. Furthermore, other techniques such as attenuation and speed of sound estimation are already implemented in clinical devices, but there is a limited number of recent studies employing them for oncology. To make this technology more widely available and accessible, standardization of QUS biomarkers and techniques is essential. Such an effort, which has already been done in other fields like liver diseases, would facilitate the clinical use of QUS in oncology, providing a more reliable treatment that is both system and operator-independent. Moreover, the field of QUS is not indifferent to the emergence of AI in the past few years, with several studies reporting the use of machine and deep learning methods for tissue characterization or QUS image reconstruction. The synergy between QUS and AI could revolutionize this field, tackling some of its limitations and accelerating the widespread implementation of these techniques in clinical settings.

REFERENCES

[1] K. Doi, "Diagnostic imaging over the last 50 years: research and development in medical imaging science and technology," *Physics in Medicine & Biology*, vol. 51, no. 13, p. R5, 2006.

[2] R. Hershkovitz, E. Sheiner, and M. Mazor, "Ultrasound in obstetrics: a review of safety," *European Journal of Obstetrics & Gynecology and Reproductive Biology*, vol. 101, no. 1, pp. 15–18, 2002.

[3] K. Paušek, "Ultrasound in diagnosis of lesions in musculoskeletal system," Ph.D. dissertation, University of Zagreb. School of Medicine, 2017.

[4] É. Cardinal, R. K. Chhem, and C. G. Beauregard, "Ultrasound-guided interventional procedures in the musculoskeletal system," *Radiologic clinics of North America*, vol. 36, no. 3, pp. 597–604, 1998.

[5] S. Bianchi, C. Martinoli, S. Bianchi, and M. P. Zamorani, "Us-guided interventional procedures," *Ultrasound of the musculoskeletal system*, pp. 891–917, 2007.

[6] F. Prada, M. Del Bene, G. Mauri, M. Lamperti, D. Vailati, C. Richetta, M. Saini, D. Santuari, M. Y. S. Kalani, and F. DiMeco, "Dynamic assessment of venous anatomy and function in neurosurgery with real-time intraoperative multimodal ultrasound," *Neurosurgical Focus*, vol. 45, no. 1, p. E6, 2018.

[7] G. Cloutier, F. Destrempes, F. Yu, and A. Tang, "Quantitative ultrasound imaging of soft biological tissues: a primer for radiologists and medical physicists," *Insights into Imaging*, vol. 12, pp. 1–20, 2021.

[8] M. L. Oelze and J. Mamou, "Review of quantitative ultrasound: Envelope statistics and backscatter coefficient imaging and contributions to diagnostic ultrasound," *IEEE transactions on ultrasonics, ferroelectrics, and frequency control*, vol. 63, no. 2, pp. 336–351, 2016.

[9] A. M. Pirmoazen, A. Khurana, A. El Kaffas, and A. Kamaya, "Quantitative ultrasound approaches for diagnosis and monitoring hepatic steatosis in nonalcoholic fatty liver disease," *Theranostics*, vol. 10, no. 9, p. 4277, 2020.

[10] T. Yamaguchi, "Basic concept and clinical applications of quantitative ultrasound (qus) technologies," *Journal of Medical Ultrasonics*, pp. 1–12, 2021.

[11] D. T. Fetzer, I. M. Rosado-Mendez, M. Wang, M. L. Robbin, A. Ozturk, K. A. Wear, J. Ormachea, T. A. Stiles, J. B. Fowlkes, T. J. Hall *et al.*, "Pulse-echo quantitative us biomarkers for liver steatosis: toward technical standardization," *Radiology*, vol. 305, no. 2, pp. 265–276, 2022.

[12] Q. W. Guerrero, H. Feltovich, I. M. Rosado-Mendez, L. C. Carlson, and T. J. Hallcor, "Quantitative ultrasound biomarkers based on backscattered acoustic power: potential for quantifying remodeling of the human cervix during pregnancy," *Ultrasound in medicine & biology*, vol. 45, no. 2, pp. 429–439, 2019.

[13] Q. Grimal and P. Laugier, "Quantitative ultrasound assessment of cortical bone properties beyond bone mineral density," *Irbm*, vol. 40, no. 1, pp. 16–24, 2019.

[14] S. J. Sanabria, E. Ozkan, M. Rominger, and O. Goksel, "Spatial domain reconstruction for imaging speed-of-sound with pulse-echo ultrasound: simulation and in vivo study," *Physics in Medicine & Biology*, vol. 63, no. 21, p. 215015, Oct. 2018, publisher: IOP Publishing, doi:10.1088/1361-6560/aae2fb.

[15] S. Flax and M. O'Donnell, "Phase-aberration correction using signals from point reflectors and diffuse scatterers: basic principles," *IEEE Transactions on Ultrasonics, Ferroelectrics, and Frequency Control*, vol. 35, no. 6, pp. 758–767, Nov. 1988, conference Name: IEEE Transactions on Ultrasonics, Ferroelectrics, and Frequency Control, doi:10.1109/58.9333.

[16] N. Hayashi, N. Tamaki, M. Senda, K. Yamamoto, Y. Yonekura, K. Torizuka, T. Ogawa, K. Katakura, C. Umemura, and M. Kodama, "A new method of measuring in vivo sound speed in the reflection mode," *Journal of Clinical Ultrasound*, vol. 16, no. 2, pp. 87–93, 1988, _eprint: https://onlinelibrary.wiley.com/doi/pdf/10.1002/jcu.1870160204, doi:10.1002/jcu.1870160204.

[17] K. Hollman, K. Rigby, and M. O'Donnell, "Coherence factor of speckle from a multi-row probe," in *1999 IEEE Ultrasonics Symposium. Proceedings. International Symposium (Cat. No.99CH37027)*, vol. 2, Oct. 1999, pp. 1257–1260 vol.2, iSSN: 1051-0117, doi:10.1109/ULTSYM.1999.849225.

[18] C. Yoon, J. Kang, S. Han, Y. Yoo, T.-K. Song, and J. H. Chang, "Enhancement of photoacoustic image quality by sound speed correction: ex vivo evaluation," *Optics Express*, vol. 20, no. 3, pp. 3082–3090, Jan. 2012, publisher: Optica Publishing Group, doi:10.1364/OE.20.003082.

[19] M. Jaeger, G. Held, S. Peeters, S. Preisser, M. Grünig, and M. Frenz, "Computed Ultrasound Tomography in Echo Mode for Imaging Speed of Sound Using Pulse-Echo Sonography: Proof of Principle," *Ultrasound in Medicine & Biology*, vol. 41, no. 1, pp. 235–250, Jan. 2015, doi:10.1016/j.ultrasmedbio.2014.05.019.

[20] N. Duric, P. Littrup, L. Poulo, A. Babkin, R. Pevzner, E. Holsapple, O. Rama, and C. Glide, "Detection of breast cancer with ultrasound tomography: First results with the Computed Ultrasound Risk Evaluation (CURE) prototype," *Medical Physics*, vol. 34, no. 2, pp. 773–785, 2007, _eprint: https://onlinelibrary.wiley.com/doi/pdf/10.1118/1.2432161, doi:10.1118/1.2432161.

[21] C. Li, N. Duric, P. Littrup, and L. Huang, "In vivo Breast Sound-Speed Imaging with Ultrasound Tomography," *Ultrasound in Medicine & Biology*, vol. 35, no. 10, pp. 1615–1628, Oct. 2009, doi:10.1016/j.ultrasmedbio.2009.05.011.

[22] N. Duric, N. Boyd, P. Littrup, M. Sak, L. Myc, C. Li, E. West, S. Minkin, L. Martin, M. Yaffe, S. Schmidt, M. Faiz, J. Shen, O. Melnichouk, Q. Li, and T. Albrecht, "Breast density measurements with ultrasound tomography: A comparison with film and digital mammography," *Medical Physics*, vol. 40, no. 1, p. 013501, 2013, _eprint: https://onlinelibrary.wiley.com/doi/pdf/10.1118/1.4772057, doi:10.1118/1.4772057.

[23] J. Wiskin, B. Malik, R. Natesan, and M. Lenox, "Quantitative assessment of breast density using transmission ultrasound tomography," *Medical Physics*, vol. 46, no. 6, pp. 2610–2620, 2019, _eprint: https://onlinelibrary.wiley.com/doi/pdf/10.1002/mp.13503, doi:10.1002/mp.13503.

[24] L. Ruby, S. J. Sanabria, K. Martini, K. J. Dedes, D. Vorburger, E. Oezkan, T. Frauenfelder, O. Goksel, and M. B. Rominger, "Breast Cancer Assessment With Pulse-Echo Speed of Sound Ultrasound From Intrinsic Tissue Reflections: Proof-of-Concept," *Investigative Radiology*, vol. 54, no. 7, p. 419, Jul. 2019, doi:10.1097/RLI.0000000000000553.

[25] H. Tanoue, Y. Urata, Y. Hagiwara, and Y. Saijo, "Sound Speed Measurement in Prostatic Cancer by Ultrasound Speed Microscope," in *Acoustical Imaging*, ser. Acoustical Imaging, A. Nowicki, J. Litniewski, and T. Kujawska, Eds. Dordrecht: Springer Netherlands, 2012, pp. 331–337, doi:10.1007/978-94-007-2619-2$_3$2.

[26] R. Seifabadi, A. Cheng, B. Malik, S. Kishimoto, J. Wiskin, J. Munasinghe, A. H. Negussie, I. Bakhutashvili, M. C. Krishna, P. Choyke, P. Pinto, A. Rahmim, E. M. Boctor, M. Merino, M. Lenox, B. Turkbey, and B. J. Wood, "Correlation of ultrasound tomography to MRI and pathology for the detection of prostate cancer," in *Medical Imaging 2019: Ultrasonic Imaging and Tomography*, vol. 10955. SPIE, Mar. 2019, pp. 77–85. [Online]. Available: https://www.spiedigitallibrary.org/conference-proceedings-of-spie/10955/109550C/Correlation-of-ultrasound-tomography-to-MRI-and-pathology-for-the/10.1117/12.2512001.full. doi:10.1117/12.2512001

[27] K. Kratkiewicz, A. Pattyn, N. Alijabbari, and M. Mehrmohammadi, "Ultrasound and Photoacoustic Imaging of Breast Cancer: Clinical Systems, Challenges, and Future Outlook," *Journal of Clinical Medicine*, vol. 11, no. 5, p. 1165, Jan. 2022, number: 5 Publisher: Multidisciplinary Digital Publishing Institute, doi:10.3390/jcm11051165.

[28] A. Popa, R. Şirli, A. Popescu, V. Bâldea, R. Lupuşoru, F. Bende, R. Cotrău, and I. Sporea, "Ultrasound-based quantification of fibrosis and steatosis with a new software considering transient elastography as reference in patients with chronic liver diseases," *Ultrasound in Medicine & Biology*, vol. 47, no. 7, pp. 1692–1703, 2021.

[29] J. Mamou and M. L. Oelze, *Quantitative ultrasound in soft tissues*. Springer, 2013.

[30] M. Linzer, *Ultrasonic Tissue Characterization: Proceedings of a Seminar Held at the National Bureau of Standards, Gaithersburg, Md., May 28-30, 1975*. U.S. Department of Commerce, National Bureau of Standards, 1976, google-Books-ID: q4BEvlTqDIYC.

[31] U. M. Pal, A. Nayak, T. Medisetti, G. Gogoi, H. Shekhar, M. Prasad, J. S. Vaidya, and H. J. Pandya, "Hybrid Spectral-IRDx: Near-IR and Ultrasound Attenuation System for Differentiating Breast Cancer From Adjacent Normal Tissue," *IEEE Transactions on Biomedical Engineering*, vol. 68, no. 12, pp. 3554–3563, Dec. 2021, conference Name: IEEE Transactions on Biomedical Engineering, doi:10.1109/TBME.2021.3077582.

[32] J. Y. Chapelon, M. Ribault, A. Birer, F. Vernier, R. Souchon, and A. Gelet, "Treatment of localised prostate cancer with transrectal high

intensity focused ultrasound," *European Journal of Ultrasound*, vol. 9, no. 1, pp. 31–38, Mar. 1999, doi:10.1016/S0929-8266(99)00005-1.

[33] O. Zenteno, W. Ridgway, S. Sarwate, M. Oelze, and R. Lavarello, "Ultrasonic attenuation imaging in a rodent thyroid cancer model," in *2013 IEEE International Ultrasonics Symposium (IUS)*. IEEE, 2013, pp. 88–91.

[34] J. Rouyer, T. Cueva, A. Portal, T. Yamamoto, and R. Lavarello, "Attenuation coefficient estimation of the healthy human thyroid in vivo," *Physics Procedia*, vol. 70, pp. 1139–1143, 2015.

[35] A. Coila, R. Laimes, C. Salazar, J. Rouyer, G. Jimenez, J. A. Pinto, J. Guerrero, and R. Lavarello, "In vivo attenuation estimation in human thyroid nodules using the regularized spectral log difference technique: Initial pilot study," in *2017 IEEE International Ultrasonics Symposium (IUS)*. IEEE, 2017, pp. 1–4.

[36] G. Ferraioli, L. Maiocchi, M. V. Raciti, C. Tinelli, A. De Silvestri, M. Nichetti, P. De Cata, M. Rondanelli, L. Chiovato, F. Calliada *et al.*, "Detection of liver steatosis with a novel ultrasound-based technique: a pilot study using mri-derived proton density fat fraction as the gold standard," *Clinical and Translational Gastroenterology*, vol. 10, no. 10, 2019.

[37] G. Ferraioli, L. Maiocchi, G. Savietto, C. Tinelli, M. Nichetti, M. Rondanelli, F. Calliada, L. Preda, and C. Filice, "Performance of the attenuation imaging technology in the detection of liver steatosis," *Journal of Ultrasound in Medicine*, vol. 40, no. 7, pp. 1325–1332, 2021.

[38] S. K. Jeon, J. M. Lee, and I. Joo, "Clinical feasibility of quantitative ultrasound imaging for suspected hepatic steatosis: intra-and inter-examiner reliability and correlation with controlled attenuation parameter," *Ultrasound in Medicine & Biology*, vol. 47, no. 3, pp. 438–445, 2021.

[39] F. Lizzi, M. Laviola, and D. Coleman, "Tissue Signature Characterization Utilizing Frequency Domain Analysis," in *1976 Ultrasonics Symposium*, Sep. 1976, pp. 714–719, doi:10.1109/ULTSYM.1976.196776.

[40] M. F. Insana, R. F. Wagner, D. G. Brown, and T. J. Hall, "Describing small-scale structure in random media using pulse-echo ultrasound," *The Journal of the Acoustical Society of America*, vol. 87, no. 1, pp. 179–192, Jan. 1990, doi:10.1121/1.399283.

[41] A. Sadeghi-Naini, H. Suraweera, W. T. Tran, F. Hadizad, G. Bruni, R. F. Rastegar, B. Curpen, and G. J. Czarnota, "Breast-Lesion Characterization using Textural Features of Quantitative Ultrasound Parametric Maps," *Scientific Reports*, vol. 7, no. 1, p. 13638, Oct. 2017, number: 1 Publisher: Nature Publishing Group, doi:10.1038/s41598-017-13977-x.

[42] N. I. Nizam, S. R. Ara, and M. K. Hasan, "Classification of breast lesions using quantitative ultrasound biomarkers," *Biomedical Signal Processing and Control*, vol. 57, p. 101786, Mar. 2020, doi:10.1016/j.bspc.2019.101786.

[43] D. Bhardwaj, A. Dasgupta, D. DiCenzo, S. Brade, K. Fatima, K. Quiaoit, M. Trudeau, S. Gandhi, A. Eisen, F. Wright, N. Look-Hong, B. Curpen, L. Sannachi, and G. J. Czarnota, "Early Changes in Quantitative Ultrasound Imaging Parameters during Neoadjuvant Chemotherapy to Predict Recurrence in Patients with Locally Advanced Breast Cancer," *Cancers*, vol. 14, no. 5, p. 1247, Jan. 2022, number: 5 Publisher: Multidisciplinary Digital Publishing Institute, doi:10.3390/cancers14051247.

[44] D. Sharma, L. O. Osapoetra, M. Faltyn, A. Giles, M. Stanisz, and G. J. Czarnota, "In vivo assessment of prostate cancer response using quantitative ultrasound characterization of ultrasonic scattering properties," *BMC Cancer*, vol. 21, no. 1, p. 991, Sep. 2021, doi:10.1186/s12885-021-08706-7.

[45] D. Rohrbach, B. Wodlinger, J. Wen, J. Mamou, and E. Feleppa, "High-Frequency Quantitative Ultrasound for Imaging Prostate Cancer Using a Novel Micro-Ultrasound Scanner," *Ultrasound in Medicine & Biology*, vol. 44, no. 7, pp. 1341–1354, Jul. 2018, doi:10.1016/j.ultrasmedbio.2018.02.014.

[46] D. Rohrbach, J. Smith, P. Goundan, H. Patel, E. J. Feleppa, and S. L. Lee, "Quantitative Ul Trasound- Based Detection of Cancerous Thyroid Nodules," in *2018 IEEE International Ultrasonics Symposium (IUS)*, Oct. 2018, pp. 1–9, iSSN: 1948-5727, doi:10.1109/ULTSYM.2018.8579930.

[47] P. N. Goundan, J. Mamou, D. Rohrbach, J. Smith, H. Patel, K. D. Wallace, E. J. Feleppa, and S. L. Lee, "A Preliminary Study of Quantitative Ultrasound for Cancer-Risk Assessment of Thyroid Nodules," *Frontiers in Endocrinology*, vol. 12, 2021.

[48] W. T. Tran, H. Suraweera, K. Quaioit, D. Cardenas, K. X. Leong, I. Karam, I. Poon, D. Jang, L. Sannachi, M. Gangeh, S. Tabbarah, A. Lagree, A. Sadeghi-Naini, and G. J. Czarnota, "Predictive quantitative ultrasound radiomic markers associated with treatment response in head and neck cancer," *Future Science OA*, vol. 6, no. 1, p. FSO433, Jan. 2020, publisher: Future Science, doi:10.2144/fsoa-2019-0048.

[49] C. Hoerig, K. Wallace, M. Wu, and J. Mamou, "Classification of Metastatic Lymph Nodes In Vivo Using Quantitative Ultrasound at Clinical Frequencies," *Ultrasound in Medicine & Biology*, vol. 49, no. 3, pp. 787–801, Mar. 2023, doi:10.1016/j.ultrasmedbio.2022.10.018.

[50] Y. Labyed and A. Milkowski, "Novel method for ultrasound-derived fat fraction using an integrated phantom," *Journal of Ultrasound in Medicine*, vol. 39, no. 12, pp. 2427–2438, 2020.

[51] E. JAKEMAN, "A model for non-rayleigh sea echo," *IEEE Trans. Antennas & Propag.*, vol. 32, no. 10, pp. 1049–1984, 1984.

[52] E. Jakeman, "On the statistics of K-distributed noise," *Journal of Physics A: Mathematical and General*, vol. 13, no. 1, p. 31, Jan. 1980, doi:10.1088/0305-4470/13/1/006.

[53] M. Nakagami, "The m-Distribution—A General Formula of Intensity Distribution of Rapid Fading," in *Statistical Methods in Radio Wave Propagation*, W. C. Hoffman, Ed. Pergamon, Jan. 1960, pp. 3–36, doi:10.1016/B978-0-08-009306-2.50005-4.

[54] P. M. Shankar, V. A. Dumane, T. George, C. W. Piccoli, J. M. Reid, F. Forsberg, and B. B. Goldberg, "Classification of breast masses in ultrasonic B scans using Nakagami and K distributions," *Physics in Medicine & Biology*, vol. 48, no. 14, p. 2229, Jul. 2003, doi:10.1088/0031-9155/48/14/313.

[55] S. Muhtadi, A. Chowdhury, R. R. Razzaque, and A. Shafiullah, "Analyzing the Texture of Nakagami Parametric Images for Classification of Breast Cancer," in *2021 IEEE National Biomedical Engineering Conference (NBEC)*, Nov. 2021, pp. 100–105, doi:10.1109/NBEC53282.2021.9618762.

[56] A. Chowdhury, R. R. Razzaque, S. Muhtadi, A. Shafiullah, E. Ul Islam Abir, B. S. Garra, and S. Kaisar Alam, "Ultrasound classification of breast masses using a comprehensive Nakagami imaging and machine learning framework," *Ultrasonics*, vol. 124, p. 106744, Aug. 2022, doi:10.1016/j.ultras.2022.106744.

[57] T. Xiao, W. Shen, Q. Wang, G. Wu, J. Yu, and L. Cui, "The detection of prostate cancer based on ultrasound RF signal," *Frontiers in Oncology*, vol. 12, 2022.

[58] M. L. Montero, O. Zenteno, B. Castaneda, M. Oelze, and R. Lavarello, "Evaluation of classification strategies using quantitative ultrasound markers and a thyroid cancer rodent model," in *2014 IEEE International Ultrasonics Symposium*, Sep. 2014, pp. 1916–1919, iSSN: 1051-0117, doi:10.1109/ULTSYM.2014.0476.

[59] J. Mamou, A. Coron, M. L. Oelze, E. Saegusa-Beecroft, M. Hata, P. Lee, J. Machi, E. Yanagihara, P. Laugier, and E. J. Feleppa, "Three-Dimensional High-Frequency Backscatter and Envelope Quantification of Cancerous Human Lymph Nodes," *Ultrasound in Medicine & Biology*, vol. 37, no. 3, pp. 345–357, Mar. 2011, doi:10.1016/j.ultrasmedbio.2010.11.020.

[60] T. M. Bui, A. Coron, J. Mamou, E. Saegusa-Beecroft, T. Yamaguchi, E. Yanagihara, J. Machi, S. L. Bridal, and E. J. Feleppa, "Modeling the envelope statistics of three-dimensional high-frequency ultrasound echo signals from dissected human lymph nodes," *Japanese Journal of Applied Physics*, vol. 53, no. 7S, p. 07KF22, Jun. 2014, publisher: IOP Publishing, doi:10.7567/JJAP.53.07KF22.

[61] P.-H. Tsui, M.-C. Ho, D.-I. Tai, Y.-H. Lin, C.-Y. Wang, and H.-Y. Ma, "Acoustic structure quantification by using ultrasound nakagami imaging for assessing liver fibrosis," *Scientific reports*, vol. 6, no. 1, p. 33075, 2016.

[62] H. Taleghamar, S. A. Jalalifar, G. J. Czarnota, and A. Sadeghi-Naini, "Deep learning of quantitative ultrasound multi-parametric images at pre-treatment to predict breast cancer response to chemotherapy," *Scientific Reports*, vol. 12, no. 1, p. 2244, Feb. 2022, number: 1 Publisher: Nature Publishing Group, doi:10.1038/s41598-022-06100-2.

[63] D. DiCenzo, K. Quiaoit, K. Fatima, D. Bhardwaj, L. Sannachi, M. Gangeh, A. Sadeghi-Naini, A. Dasgupta, M. C. Kolios, M. Trudeau, S. Gandhi, A. Eisen, F. Wright, N. Look Hong, A. Sahgal, G. Stanisz, C. Brezden, R. Dinniwell, W. T. Tran, W. Yang, B. Curpen, and G. J. Czarnota, "Quantitative ultrasound radiomics in predicting response to neoadjuvant chemotherapy in patients with locally advanced breast cancer: Results from multi-institutional study," *Cancer Medicine*, vol. 9, no. 16, pp. 5798–5806, 2020, _eprint: https://onlinelibrary.wiley.com/doi/pdf/10.1002/cam4.3255, doi:10.1002/cam4.3255.

[64] M. Bernhardt, V. Vishnevskiy, R. Rau, and O. Goksel, "Training Variational Networks With Multidomain Simulations: Speed-of-Sound Image Reconstruction," *IEEE Transactions on Ultrasonics, Ferroelectrics, and Frequency Control*, vol. 67, no. 12, pp. 2584–2594, Dec. 2020, conference Name: IEEE Transactions on Ultrasonics, Ferroelectrics, and Frequency Control, doi:10.1109/TUFFC.2020.3010186.

[65] M. Heller and G. Schmitz, "Deep Learning-based Speed-of-Sound Reconstruction for Single-Sided Pulse-Echo Ultrasound using a Coherency Measure as Input Feature," in *2021 IEEE International Ultrasonics Symposium (IUS)*, Sep. 2021, pp. 1–4, iSSN: 1948-5727, doi:10.1109/IUS52206.2021.9593406.